Dual oxidase 1 promotes antiviral innate immunity

Demba Sarr[a,1], Aaron D. Gingerich[a,1], Nuha Milad Asthiwi[a], Faris Almutairi[a,b], Giuseppe A. Sautto[c], Jeffrey Ecker[c], Tamás Nagy[d], Matthew B. Kilgore[e,f], Joshua D. Chandler[e,f], Ted M. Ross[a,c], Ralph A. Tripp[a], and Balázs Rada[a,2]

[a]Department of Infectious Diseases, College of Veterinary Medicine, University of Georgia, Athens, GA 30602; [b]Department of Pharmaceutical and Biomedical Sciences, College of Pharmacy, University of Georgia, Athens, GA 30602; [c]Center for Vaccines and Immunology, University of Georgia, Athens, GA 30602; [d]Department of Pathology, College of Veterinary Medicine, University of Georgia, Athens, GA 30602; [e]Department of Pediatrics, Division of Pulmonary, Allergy and Immunology, Cystic Fibrosis, and Sleep Medicine, Emory University School of Medicine, Atlanta, GA 30322; and [f]Center for Cystic Fibrosis and Airways Disease Research, Children's Healthcare of Atlanta, Atlanta, GA 30322

Edited by Vishva M. Dixit, Genentech, San Francisco, CA, and approved May 15, 2021 (received for review August 12, 2020)

Dual oxidase 1 (DUOX1) is an NADPH oxidase that is highly expressed in respiratory epithelial cells and produces H_2O_2 in the airway lumen. While a line of prior in vitro observations suggested that DUOX1 works in partnership with an airway peroxidase, lactoperoxidase (LPO), to produce antimicrobial hypothiocyanite ($OSCN^-$) in the airways, the in vivo role of DUOX1 in mammalian organisms has remained unproven to date. Here, we show that Duox1 promotes antiviral innate immunity in vivo. Upon influenza airway challenge, *Duox1*$^{-/-}$ mice have enhanced mortality, morbidity, and impaired lung viral clearance. Duox1 increases the airway levels of several cytokines (IL-1β, IL-2, CCL1, CCL3, CCL11, CCL19, CCL20, CCL27, CXCL5, and CXCL11), contributes to innate immune cell recruitment, and affects epithelial apoptosis in the airways. In primary human tracheobronchial epithelial cells, $OSCN^-$ is generated by LPO using DUOX1-derived H_2O_2 and inactivates several influenza strains in vitro. We also show that $OSCN^-$ diminishes influenza replication and viral RNA synthesis in infected host cells that is inhibited by the H_2O_2 scavenger catalase. Binding of the influenza virus to host cells and viral entry are both reduced by $OSCN^-$ in an H_2O_2-dependent manner in vitro. $OSCN^-$ does not affect the neuraminidase activity or morphology of the influenza virus. Overall, this antiviral function of Duox1 identifies an in vivo role of this gene, defines the steps in the infection cycle targeted by $OSCN^-$, and proposes that boosting this mechanism in vivo can have therapeutic potential in treating viral infections.

DUOX1 | Dual oxidase 1 | influenza | hypothiocyanite | lactoperoxidase

DUOX1 is one of the seven members of the NADPH oxidase enzyme family (1). DUOX1 was first described in the thyroid gland (2) but was later also detected in several other tissues and organs including the tracheobronchial epithelium (3). DUOX1 localizes to the apical plasma membrane of ciliated respiratory epithelial cells and produces extracellular H_2O_2 into the airway lumen in a Ca^{2+}-dependent manner (3, 4). DUOX1 is the major NADPH oxidase expressed and the main source of H_2O_2 in the airway epithelium (3, 5, 6).

The respiratory epithelium employs several immune mechanisms against airborne microbes including the generation of reactive oxygen species. Respiratory epithelial cells have a proposed, rapid oxidative and extracellular antimicrobial system consisting of LPO, thiocyanate (SCN^-), and hydrogen peroxide (H_2O_2) (7–10). LPO is found in a variety of body fluids including milk, saliva, lachrymal, and airway secretions (7, 8, 10–13). Its main substrate, SCN^-, is abundant in the airway surface liquid (7, 9, 14). LPO oxidizes SCN^- into antimicrobial hypothiocyanite ($OSCN^-$) using H_2O_2 (15). Prior in vitro data suggested that Duox1 is the epithelial H_2O_2 source that functions in partnership with LPO to produce antimicrobial $OSCN^-$(2, 3, 16). SCN^- supplementation increases bacterial clearance in mouse lung infection, supporting an antibacterial role of $OSCN^-$ in vivo (17, 18). While $OSCN^-$ kills several microorganisms in vitro, its mechanism of action and the identity of the in vivo H_2O_2 source required to generate $OSCN^-$ remained unknown. The in vivo role of Duox1 in mammals remained unproven to date (13, 19).

Influenza remains a major clinical challenge worldwide. Seasonal influenza viruses infect between three and five million people and cause 290,000 to 650,000 global deaths annually (20). In this study, we show that Duox1 promotes innate immunity in vivo against influenza infection in a mouse model. We also identify virus binding and entry into host cells as the basis for the antiviral mechanism of action of $OSCN^-$ in vitro. Overall, results shown here demonstrate the in vivo role of Duox1 and determine the steps in the influenza virus life cycle targeted by Duox1- and LPO-derived $OSCN^-$.

Results

Duox1 Improves Mortality, Morbidity, and Viral Clearance in a Murine Model of Influenza Airway Infection. We have previously shown that $OSCN^-$ produced by the Duox1/LPO-based system in vitro inactivates several influenza A and B virus strains (21, 22). To explore the in vivo role of Duox1 in anti-influenza responses, *Duox1*$^{-/-}$ mice (23) and Duox1-expressing C57BL/6 wild-type control animals (WT) (*SI Appendix*, Fig. S1*A*) were intranasally (i.n.) infected with 50 plaque-forming units (PFUs) of mouse-adapted influenza A virus strain, A/Puerto Rico/8/1934 (H1N1) (PR8). While 86% of WT mice survived the i.n. influenza challenge at day 12, only 55% of the *Duox1*$^{-/-}$ mice survived ($\chi^2 = 5.3$, $P = 0.02$) (Fig. 1*A*). *Duox1*$^{-/-}$ mice lost significantly more body weight compared with WT mice ($P < 0.05$, 5 through 7 d postinfection, dpi) (Fig. 1 *B* and *C*) during the time before the onset of mortality. The improved

Significance

Influenza infections kill millions of people worldwide. Current prophylactic treatment options are limited due to viral strain–specific vaccinations and emerging drug resistance. It is important to discover new immune mechanisms that can fight the influenza virus. Our work presented here identifies such a mechanism. The Duox1 protein helps the airways to clear influenza virus and to reduce infection-related death and sickness in an animal model. Duox1 delays the infection process by directly targeting the virus. Unlike current vaccines, this mechanism is effective against several influenza strains. Our study identifies the function of the *Duox1* gene and suggests that it has a therapeutic potential against influenza and potentially other respiratory pathogens, worth exploring in the future.

Author contributions: D.S., A.D.G., R.A.T., and B.R. designed research; D.S., A.D.G., N.M.A., F.A., G.A.S., J.E., T.N., M.B.K., J.D.C., and B.R. performed research; G.A.S. contributed new reagents/analytic tools; D.S., A.D.G., N.M.A., F.A., G.A.S., J.E., T.N., J.D.C., and B.R. analyzed data; and D.S., A.D.G., T.M.R., R.A.T., and B.R. wrote the paper.

The authors declare no competing interest.

This article is a PNAS Direct Submission.

[1]D.S. and A.D.G. contributed equally to this work.

[2]To whom correspondence may be addressed. Email: radab@uga.edu.

This article contains supporting information online at https://www.pnas.org/lookup/suppl/doi:10.1073/pnas.2017130118/-/DCSupplemental.

Published June 24, 2021.

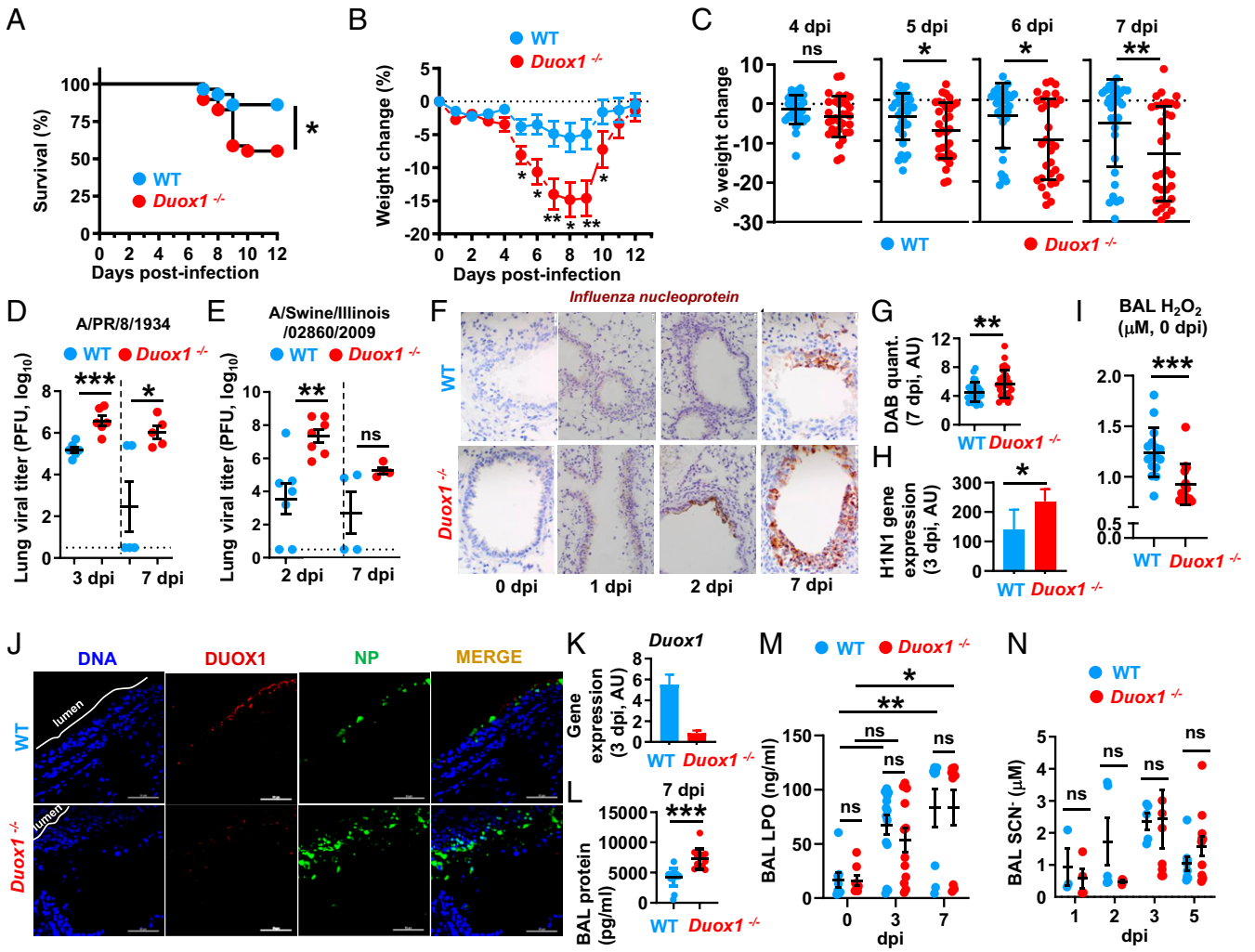

Fig. 1. Duox1$^{-/-}$ mice demonstrate increased mortality, morbidity, and impaired viral clearance following influenza airway infection. (*A*) Kaplan–Meier survival curves of *Duox1*$^{-/-}$ ($n = 28$) and WT ($n = 29$) mice infected i.n. with A/Puerto Rico/8/1934 (H1N1) (PR8) influenza strain (50 PFU) followed for 12 d (chi-square test). Weight loss of *Duox1*$^{-/-}$ and WT mice infected as in *A* is presented as *B*, the daily average for the 12-d duration of the study or (*C*) individual animal data on 4 to 7 dpi, before and on the day of the onset of mortality on 8 dpi (Mann–Whitney *U* test). *Duox1*$^{-/-}$ and WT mice were infected i.n. with (*D*) PR8 (50 PFU) or (*E*) the nonlethal A/Swine/Illinois/02860/2009 H1N2 (10^5 PFU) influenza virus strain, and viral titers in whole-lung homogenates were determined using PFU assay on MDCK cells at the indicated time points. The dotted lines indicate the limit of detection of the assay (unpaired *t* test). (*F*) Influenza virus NP expression was measured by immunohistochemistry in the lungs of *Duox1*$^{-/-}$ and WT mice infected i.n. with PR8. Representative images ($n = 10$ WT and $n = 15$ *Duox1*$^{-/-}$ mice) are shown. (*G*) Quantification of influenza NP expression determined as in *F* in *Duox1*$^{-/-}$ and WT mice 7 dpi using the Fiji software ($n = 10$ WT and $n = 15$ *Duox1*$^{-/-}$ mice) (Mann–Whitney *U* test). (*H*) Gene expression of H1N1 influenza virus was determined in the lungs of WT and *Duox1*$^{-/-}$ animals by qPCR. Bar graphs display mean. $n = 7$. (*I*) Quantification of H_2O_2 concentrations in the BAL of uninfected *Duox1*$^{-/-}$ ($n = 14$) and *WT* ($n = 16$) mice by Amplex Red fluorescence (Mann–Whitney *U* test). (*J*) *Duox1*$^{-/-}$ and WT mice were i.n. infected with PR8 (50 PFU) as in *A*, lungs were fixed, and immunofluorescence staining was performed using an anti-DUOX1 antibody (red), an anti-NP antibody identifying influenza virus NP (green), and DAPI (blue) to detect DNA. Merged images indicate the overlay of red, green, and blue. The white line and text "lumen" on the blue images indicate the border between the airway lumen and the epithelium. (Scale bars, 20 μm.) (*K*) Gene expression of *Duox1* was measured in the lungs of WT and *Duox1*$^{-/-}$ animals by qPCR. Bar graphs display mean. $n = 3$. (*L*) Total protein levels were determined in the BAL of PR8-infected ($n = 9$ WT and $n = 5$ *Duox1*$^{-/-}$) mice on 7 dpi using the BCA assay (Mann–Whitney *U* test). (*M*) *Duox1*$^{-/-}$ and WT mice were either uninfected (0 dpi) or i.n. infected with PR8 (50 PFU), and BAL concentrations of LPO were determined by ELISA at indicated days ($n = 32$ WT, $n = 30$ *Duox1*$^{-/-}$ animals with a minimum number of 8 mice per day). (*N*) SCN^- concentrations were determined by mass spectrometry in BAL fluid of PR8-infected mice ($n = 28$ WT and $n = 21$ *Duox1*$^{-/-}$, with a minimum number of 4 mice per time point) throughout the infection (1 to 5 dpi). Significance levels are indicated as $^*P < 0.05$, $^{**}P < 0.01$, and $^{***}P < 0.001$. Abbreviations: AU, arbitrary unit; BAL, bronchoalveolar lavage; DAB, 3,3′-diaminobenzidine; dpi, day postinfection; Duox1, Dual oxidase 1; i.n., intranasally; LPO, lactoperoxidase; NP, nucleoprotein; ns, nonsignificant; PFU, plaque-forming unit; SCN^-, thiocyanate; WT, wild-type.

body weight after day 8 reflects the recovery of the surviving animals. The viral loads in the lungs of *Duox1*$^{-/-}$ mice were significantly higher compared with WT mice on 3 ($P < 0.001$) and 7 dpi ($P < 0.05$) (Fig. 1*D*). To confirm that this antiviral effect was not virus strain specific, WT and *Duox1*$^{-/-}$ mice were i.n. infected with a nonlethal dose (10^5 PFU) of an $OSCN^-$-sensitive influenza strain, A/swine/Illinois/02860/09 (H1N2) (21). Similar to PR8-challenged mice, lung viral loads in *Duox1*$^{-/-}$ mice challenged with the H1N2 influenza strain were significantly higher compared with WT mice ($P < 0.05$, 2 dpi) (Fig. 1*E*). To further evaluate the effects of airway Duox1 on viral replication, lungs from PR8-infected mice were sectioned and probed with anti-nucleoprotein (NP) antibody. Influenza NP was detected by immunohistochemistry mainly in the bronchial epithelium (Fig. 1*F*), and its quantification resulted in a significantly elevated signal in *Duox1*$^{-/-}$ mice compared with WT controls at 7 dpi ($P < 0.01$) (Fig. 1*G*). Viral gene expression was also

higher in *Duox1*$^{-/-}$ lungs (Fig. 1*H*). H_2O_2 concentrations in the bronchoalveolar lavage fluid (BAL) of uninfected WT mice (1.23 ± 0.06 μM, mean ± SEM, $n = 16$) were significantly elevated compared with those observed in *Duox1*$^{-/-}$ animals (0.92 ± 0.05 μM, mean ± SEM, $n = 14$) (Fig. 1*I*). Increased PR8 viral load in *Duox1*$^{-/-}$ airways was further confirmed by immunofluorescence detection of NP (Fig. 1*J*). These results suggest that Duox1 is a major contributor to airway H_2O_2 production in mice, and H_2O_2 production by Duox1 helps to control influenza A virus replication and promotes viral clearance in the airways.

Next, we investigated whether Duox1 affected BAL levels of the other components of the Duox1/LPO/SCN$^-$ system. Duox1 is the principal Duox isoform expressed in the trachea and lungs of uninfected WT mice (*SI Appendix*, Fig. S1*B*). As expected, *Duox1* messenger RNA (mRNA) was not detected in *Duox1*$^{-/-}$ mice (Fig. 1*K*). Duox1 protein expression assessed by immunofluorescence was absent in *Duox1*$^{-/-}$ mice but was present in WT airways at 3 and 7 dpi (Fig. 1*J* and *SI Appendix*, Fig. S1*C*). To confirm the specificity of the used antibody toward Duox1, we also examined thyroid glands known to express both Duox isoforms (24) and found that Duox1 was detected by immunofluorescence in the thyroid glands of WT mice only but not in *Duox1*$^{-/-}$ mice (*SI Appendix*, Fig. S1*D*).

Total protein levels in the BAL supernatants evaluated as a measure of the general inflammatory response and epithelial leakage were significantly elevated in *Duox1*$^{-/-}$ mice compared with WT controls (Fig. 1*L*). Our group recently showed LPO expression in the murine respiratory tract (13). LPO levels in the BAL measured by enzyme-linked immunosorbent assay (ELISA) were not different at any time point examined between WT or *Duox1*$^{-/-}$ mice but considerably increased following influenza virus infection (Fig. 1*M*). SCN$^-$ levels in the BAL fluid of WT and

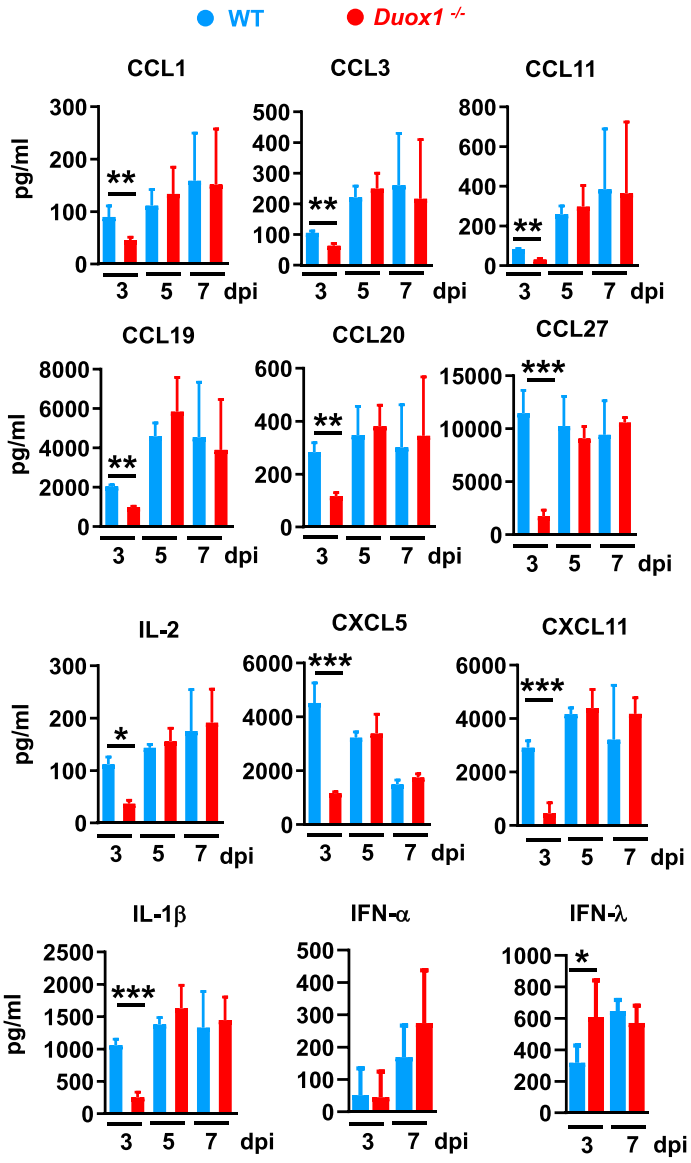

Fig. 2. *Duox1*$^{-/-}$ mice have an altered cytokine response following influenza lung infection. Concentrations of indicated cytokines/chemokines in the BAL of WT ($n = 19$) and *Duox1*$^{-/-}$ mice ($n = 20$) infected with the A/Puerto Rico/8/1934 (H1N1) (PR8) influenza virus strain (50 PFU) were determined by a multiplex bead-based ELISA array or classical, microplate-based ELISAs (IFN-α, IFN-λ) at 3, 5, and 7 dpi. Data are presented as mean ± SEM. Statistical comparisons were done with Mann–Whitney *U* test at each dpi between *Duox1*$^{-/-}$ and WT mice. Significance levels are indicated as $^*P < 0.05$, $^{**}P < 0.01$, and $^{***}P < 0.001$. Abbreviations: dpi, day postinfection; Duox1, Dual oxidase 1; WT, wild-type.

Duox1$^{-/-}$ mice were determined by mass spectrometry at 1, 2, 3, and 5 dpi, but no significant differences were detected (Fig. 1*N*). These results show that the absence of *Duox1* does not affect the components required for $OSCN^-$ generation besides H_2O_2.

Duox1 Shapes the Early Cytokine Response to Influenza in the Lung. To characterize the role of Duox1 in the immune response to influenza virus infection, pro- and anti-inflammatory cytokines in the BAL of WT and *Duox1*$^{-/-}$ mice were quantified at days 3, 5, and 7 post-PR8 infections. At 3 dpi, the data reveal considerably higher cytokine (IL-1β and IL-2) and chemokine (CCL1, CCL3, CCL11, CCL19, CCL20, CCL27, CXCL5, and CXCL11) levels in WT compared with *Duox1*$^{-/-}$ mice (Fig. 2). The most striking and significant differences in cytokine levels occurred for CCL27, IL-1β, and CXCL5 (Fig. 2), while other chemokines showed no differences between WT and *Duox1*$^{-/-}$ mice (*SI Appendix*, Fig. S2). During influenza virus infection, interferons (IFNs) regulate viral replication and promote an antiviral state of the host (25). Our data showed comparable IFN-α levels in the BAL of both WT and *Duox1*$^{-/-}$ mice (Fig. 2); however, IFN-λ levels were significantly ($P < 0.05$) higher in the BAL of *Duox1*$^{-/-}$ compared with WT mice (Fig. 2). No differences were observed in the BAL levels of any cytokines at 5 and 7 dpi (Fig. 2). These results support that Duox1 participates in shaping the initial immune response during influenza virus challenge.

We used flow cytometry to determine the nature of immune cells recruited to the BAL of influenza-infected mice at 3, 5, and 7 dpi (*SI Appendix*, Fig. S3 *A* and *B*). In uninfected mice, no significant differences were detected in leukocyte numbers in the BAL or in the spleen (*SI Appendix*, Fig. S4) between WT and *Duox1*$^{-/-}$ animals. Leukocyte numbers increased over time following influenza virus infection (*SI Appendix*, Fig. S5*A*). Myeloid cells appeared early after infection, while T cells, B cells, and NK cells peaked later, at 7 dpi (*SI Appendix*, Fig. S5*A*). The overall number of leukocytes, neutrophils, alveolar macrophages, eosinophils, T cells, and B cells was not significantly different between WT and *Duox1*$^{-/-}$ mice, except for inflammatory macrophages whose number was higher at 5 dpi in *Duox1*$^{-/-}$ animals compared with WT mice (*SI Appendix*, Fig. S5*A*). There was a trend toward lower lymphoid cell numbers at 7 dpi and higher monocyte/macrophage numbers at 5 dpi in *Duox1*$^{-/-}$ mice (*SI Appendix*, Fig. S5*A*). In the spleen, no significant differences in myeloid cell numbers were observed (*SI Appendix*, Fig. S5*B*).

Duox1 Attenuates Airway Epithelial Apoptosis following Influenza Airway Infection. To determine if *Duox1* deficiency affects lung histopathology during influenza virus infection, lungs of *Duox1*$^{-/-}$ and WT mice were examined at 0, 3, and 7 dpi. Lung sections were stained with hematoxylin and eosin and were examined by a board-certified veterinary pathologist using a light microscope. Histopathologic evaluation revealed a robust inflammatory response, particularly at 7 dpi (Fig. 3*A*). While no differences were found between WT and *Duox1*$^{-/-}$ mice in lung inflammatory histopathology scores (Fig. 3*B*), there was a qualitative difference in histopathology at 7 and 12 dpi. *Duox1*$^{-/-}$ lungs exhibited multifocal, distinct areas of type II pneumocyte hyperplasia (Fig. 3*C*). The presence of type II pneumocytes in *Duox1*$^{-/-}$ lungs signifies prior intensive damage to type I pneumocytes that was likely due to diminished resistance of bronchiolar epithelial cells to influenza virus resulting in viral access to the alveolar spaces and type I pneumocytes. Although histopathologic lesions were the most robust at 7 dpi, no difference in cytokine and chemokine expression was observed at 7 dpi. The most likely explanation for this observed phenomenon is that cytokine and chemokine expression preceded development of histopathological lesions (i.e., the development of histopathologic lesions lags behind cytokine and chemokine expression levels).

Apoptosis of airway epithelial cells results from infection by influenza virus (26); thus, we tested the impact of Duox1 on airway epithelial apoptosis following influenza virus infection. Immunofluorescence staining of the apoptotic marker, cleaved caspase-3, showed that at 3 and 7 dpi there was substantially greater epithelial cell apoptosis in *Duox1*$^{-/-}$ mice compared with WT mice (Fig. 3 *D* and *E*). No difference was observed in the levels of full-length, uncleaved caspase-3 or α-tubulin (*SI Appendix*, Fig. S6 *A* and *B*). Immunoblot analysis was also used to further confirm the increased levels of apoptosis (caspase-3 cleavage) in influenza-challenged *Duox1*$^{-/-}$ animals (Fig. 3 *F* and *G*). Duox1 deficiency did not affect α-tubulin or full-length caspase-3 (*SI Appendix*, Fig. S6*C*). The NP immunoblot signal indicative of lung viral burden was significantly enhanced in *Duox1*$^{-/-}$ mice compared with WT animals (Fig. 3*G*) and significantly correlated with the apoptotic signal (Fig. 3*H*). Enhanced apoptosis was further confirmed by terminal deoxynucleotidyl transferase dUTP nick end labeling (TUNEL) assay (Fig. 3 *I* and *J* and *SI Appendix*, Fig. S6 *D* and *E*). Overall, these data suggest that influenza virus clearance and associated airway epithelial apoptosis depend on the presence of a functional Duox1.

DUOX1-Derived H_2O_2 Promotes Influenza Virus Inactivation in Normal Human Bronchial Epithelial Cells. DUOX1 expression in the lung is the highest in the respiratory epithelium, and DUOX1 is the main source of H_2O_2 generated by respiratory epithelial cells including differentiated normal human bronchial epithelial (NHBE) cells (Fig. 4 *A* and *B*). We previously showed that the H1N2 influenza strain, A/swine/Illinois/02860/2009, is inactivated by rat tracheobronchial epithelial cells supplemented with LPO and SCN^- in a Duox1/H_2O_2-dependent manner (21). To determine whether this and other influenza strains are also inactivated by differentiated NHBE cells, NHBE cells were infected with one of the following influenza strains: A/California/07/2009 (H1N1), A/turkey/KS/4880/1980 (H1N1), A/Wisconsin/67/2005 (H3N2), and B/Florida/4/2006 Yamagata. A 1 to 2 log decrease in viral infectivity was observed when LPO and SCN^- were applied together (Fig. 4*C*). Catalase blocked the antiviral effects of $OSCN^-$ by removing the H_2O_2 substrate of LPO produced by Duox1 in the airways (Fig. 4*C*). Collectively, these data confirm that NHBE cells generate sufficient H_2O_2 to promote $OSCN^-$-mediated inactivation of several influenza virus strains and that $OSCN^-$, and not H_2O_2, is responsible for influenza virus inactivation.

LPO-Generated $OSCN^-$ Directly Targets the Influenza Virus and Reduces Viral RNA Synthesis in Host Cells. We previously demonstrated that $OSCN^-$ is sufficient to inactivate several influenza A and B strains in vitro using an experimental cell-free system where H_2O_2 generation by DUOX1 in NHBE cells is replaced by H_2O_2 production by the enzymatic reaction of glucose and glucose oxidase (22). The concentration of glucose oxidase has been optimized to result in the same H_2O_2 output as NHBE cells (6, 22). The cell-free system generates $OSCN^-$, and influenza inactivation is mediated by $OSCN^-$, not H_2O_2 (21, 27). To further address strain differences, five additional influenza strains were evaluated for their sensitivity to $OSCN^-$: A/California/07/2009 (H1N1); A/Aichi/2/1968 (H3N2); B/Brisbane/33/2008 Victoria; and B/Florida/4/2006 Yamagata. The fifth influenza strain examined is the A/Puerto Rico/8/1934 (H1N1) used in the mouse studies. All strains tested were inactivated by $OSCN^-$ in a cell-free system (22) (Fig. 4*D*).

The most commonly used antiviral drug to treat influenza infection is the neuraminidase (NA) inhibitor, oseltamivir (Tamiflu), that binds to the active site of NA inhibiting its enzymatic activity (28). Resistance has emerged against NA inhibitors (29). We tested whether the A/Mississippi/3/2001 (H1N1) H275Y influenza mutant strain that is resistant to NA inhibitors (30) (*SI Appendix*, Fig. S7) was inactivated by $OSCN^-$. Our results found that this strain

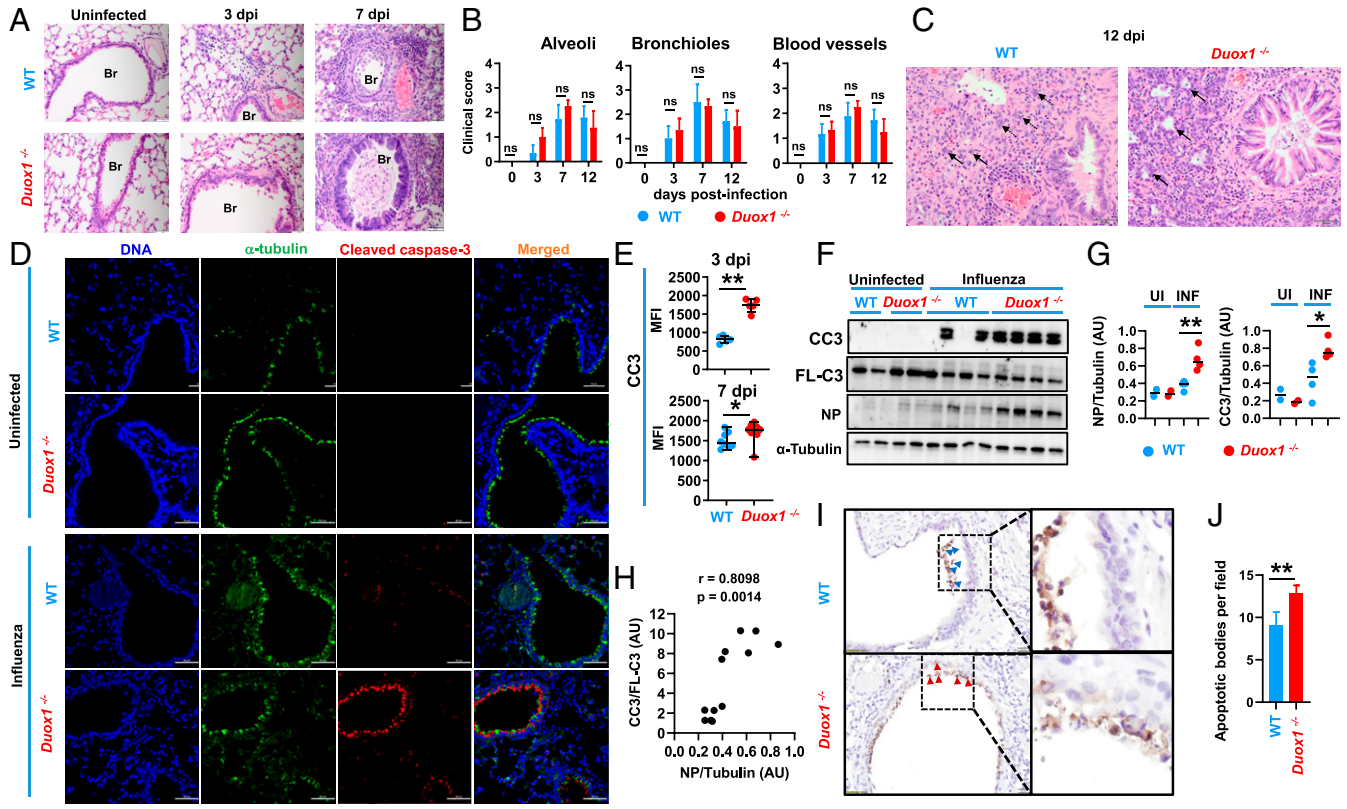

Fig. 3. Enhanced epithelial apoptosis in influenza virus–infected *Duox1*$^{-/-}$ mice. (*A*) Histopathological micrographs of hematoxylin and eosin-stained lung tissue sections of *Duox1*$^{-/-}$ and WT mice that were left uninfected or were infected i.n. with the A/Puerto Rico/8/1934 (H1N1) (PR8) influenza virus strain (50 PFU) at 3 and 7 dpi are shown. Representative images of at least five similar results are shown. Magnification: 40×. (Scale bars, 20 μm.) (*B*) Clinical scores of alveoli, bronchioles, and blood vessels in PR8-infected *Duox1*$^{-/-}$ and WT mice at 3 and 7 dpi ($n = 5$ to 12). Statistical comparisons were done by Mann–Whitney *U* test at each dpi between genotypes. (*C*) High magnification images of affected lungs in WT and *Duox1*$^{-/-}$ mice at 12 dpi. WT: The alveolar spaces are obscured due to accumulation of histiocytes (arrows) and syncytial cells (dashed arrows). There is also some residual, mostly lymphocytic inflammatory infiltrate within alveolar spaces. The histiocytes represent residual inflammation, while the syncytial cells are formed by fusion of parenchymal cells (pneumocytes). *Duox1*$^{-/-}$: The alveolar spaces are infiltrated with inflammatory cells throughout the image. There are also numerous outlines of small open areas (arrows) in the parenchyma (where the normal alveoli used to be). These open areas are lined by cuboidal epithelial cells (type II pneumocyte hyperplasia). Type II pneumocyte hyperplasia signifies a regenerative process unique to the lungs where, after necrosis of type I pneumocytes (flat epithelial cells that normally line the alveoli), type II pneumocytes (cuboidal epithelial cells) proliferate. Hematoxylin and eosin staining, 200× original magnification. (Scale bar, 50 μm.) (*D*) Representative immunofluorescence staining of cleaved caspase-3 (CC3, red), α-tubulin (green), and DAPI (blue) in uninfected (two *Top Rows*) and PR8-infected (two *Bottom Rows*, 3 dpi) WT and *Duox1*$^{-/-}$ mouse lungs ($n = 5$). (*E*) Comparative statistics of the quantitation of the immunofluorescence signals (shown in *D*) of PR8-infected *Duox1*$^{-/-}$ and WT mice at 3 and 7 dpi. Mean fluorescent intensity (MFI) ± SEM of cleaved caspase-3 (CC3, *Left*) and of α-tubulin (*Right*) immunofluorescence is shown (Mann–Whitney *U* test, $n = 5$ WT and $n = 5$ *Duox1*$^{-/-}$ mice). (*F*) Immunoblot analysis of lung lysates collected from *Duox1*$^{-/-}$ and WT mice (uninfected or infected with influenza PR8 strain 7 dpi) using specific antibodies detecting α-tubulin, viral NP, cleaved CC3 and full-length caspase-3 (FL-C3). Each column represents a separate animal. Four animals per genotype were infected with influenza, and two animals per genotype were used as uninfected controls. (*G*) Densitometry data of the immunoblot shown in *F*. Each dot represents a separate animal. One-way ANOVA, Holm–Šídák's multiple comparisons test. (*H*) Indicated densitometric ratios (NP/α-tubulin versus CC3/FLC3) were calculated from both *Duox1*$^{-/-}$ and *WT* animals and correlated with each other based on the results of the immunoblot shown in *F*. Pearson's correlation analysis. r, correlation coefficient. (*I*) TUNEL assay was used to detect apoptosis in the bronchioles of influenza-infected *Duox1*$^{-/-}$ and *WT* mice (7 dpi). One representative result is shown ($n = 7$). (*J*) Apoptotic bodies per field were counted in TUNEL-strained bronchioles of *Duox1*$^{-/-}$ and *WT* mice inflected with influenza ($n = 7$). Mann–Whitney *U* test. Significance levels are indicated as $*P < 0.05$ and $**P < 0.01$. Abbreviations: AU, arbitrary unit; Br, bronchus; CC3, cleaved caspase-3; dpi, day postinfection; Duox1, Dual oxidase 1; FL-C3, full-length caspase-3; INF, infected; MFI, mean fluorescence intensity; NP, viral nucleoprotein; ns, nonsignificant; UI, uninfected; WT, wild-type.

and its NA inhibitor-sensitive control strain (A/Mississippi/3/2001 [H1N1] 275H) were both equally inactivated by OSCN$^-$ (Fig. 4*D*).

The inhibitory action of OSCN$^-$ on influenza virus proliferation was further confirmed in Madin–Darby canine kidney (MDCK) cells by NP immunofluorescence staining 24 hpi of A/California/07/2009 (H1N1) (Fig. 4*E*). The results also showed that OSCN$^-$-mediated influenza inactivation improves at slightly acidic pH where OSCN$^-$ is known to be increasingly protonated (31) (*SI Appendix*, Fig. S8). Based on these data and those published (22), we conclude that OSCN$^-$ has a general antiviral effect against influenza strains including those resistant to currently used antivirals.

To reveal whether the antiviral effect of OSCN$^-$ is indirect, that is, functioning by priming host cells, an A/Puerto Rico/8/1934-PA-NanoLuciferase (H1N1) virus strain was examined (32). This reporter virus (PR8-NanoLuc) enables sensitive, easy, and early (8 h) detection of viral titers by chemiluminescence (Fig. 4*F*) (32). When OSCN$^-$ was generated before influenza virus (Fig. 4*G*, experimental plan, condition 2), no reduction in viral replication was seen compared with virus alone (condition 1) that was not affected by catalase (condition 3). However, when OSCN$^-$ was added concomitantly with influenza (condition 4), a considerable reduction in viral replication was observed that was blocked by catalase (condition 5) (Fig. 4*G*). These data

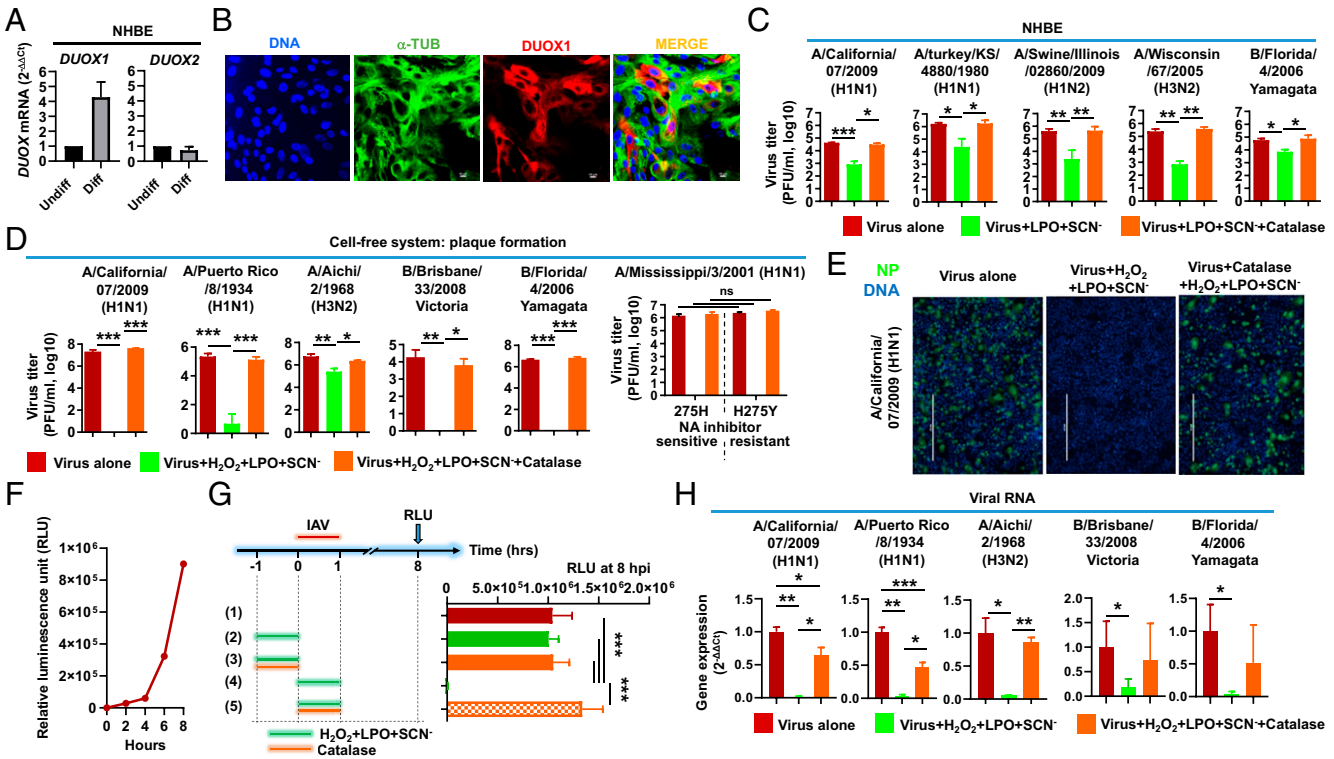

Fig. 4. $OSCN^-$ generated by LPO and DUOX1-derived H_2O_2 reduces influenza virus replication in host cells. (*A*) DUOX1 and DUOX2 mRNA expressions were measured in differentiated (diff) and undifferentiated (undiff) NHBE cells using real-time PCR. GAPDH was used as reference. Mean ± SD. (*B*) NHBE cells differentiated on air–liquid interface (ALI) were fixed and processed for immunofluorescence to detect α-tubulin (green) and DUOX1 (red) using specific antibodies. DNA is stained by DAPI (blue). One representative result of three similar ones. (*C*) ALI cultures of differentiated human NHBE cells were exposed to 5×10^4 PFUs of the indicated influenza virus strains in the presence or absence of LPO, SCN^-, or catalase in the indicated combinations. After 60 min, infectious virus titers were determined by PFU assay using MDCK cells. Data are expressed as mean ± SEM of independent experiments: A/California/07/2009 (H1N1) (n = 2), A/turkey/KS/4880/1980 (H1N1) (n = 4), A/swine/Illinois/02860/2009 (H3N2) (n = 6), A/Wisconsin/67/2005 (H3N2) (n = 3), and B/Florida/4/2006 Yamagata (n = 3), performed in duplicates. One-way ANOVA and Tukey's multiple comparisons test. (*D*) The indicated influenza virus strains were exposed to $OSCN^-$ in the cell-free system for 1 h in the presence or absence of catalase, and viral titers were determined by PFU assay on MDCK cells. Data are expressed as mean ± SEM of the following numbers of independent experiments: A/California/07/2009 (H1N1) (n = 5), A/Puerto Rico/8/1934 (H1N1) (n = 4), A/Aichi/2/1968 (H3N2) (n = 4), B/Brisbane/33/2008 Victoria (n = 2), B/Florida/4/2006 Yamagata (n = 5), the NA inhibitor (oseltamivir)-resistant influenza virus strain, A/Mississippi/3/2001 (H1N1) H275Y, and its NA inhibitor-sensitive, parental strain A/Mississippi/3/2001 (H1N1) 275H (n = 2). One-way ANOVA and Tukey's multiple comparisons tests. (*E*) The A/California/07/2009 (H1N1) strain was exposed to $OSCN^-$ for 1 h in the presence or absence of catalase in the cell-free system and transferred to MDCK cells. Cells were fixed and stained for the viral NP (green) 24 h later. DNA is detected by DAPI. One representative experiment of three similar ones is shown. (*F*) Growth curve of influenza virus A/Puerto Rico/8/1934-PA-NanoLuciferase (H1N1) (PR8-NanoLuc) in MDCK cells infected with 128 hemagglutination units (HAUs) was measured in a microplate luminometer and expressed as relative luminescence. Presented data are derived from one experiment performed in triplicates. (*G*) MDCK cells were infected with 128 HAUs of PR8-NanoLuc and exposed to $OSCN^-$ before or at the same time of viral infection, as explained in the scheme. Luminescence was measured at 8 h postinfection in a microplate luminometer. Data are expressed as mean ± SEM of n = 4 independent experiments performed in triplicates. One-way ANOVA and Tukey's multiple comparisons test. (*H*) Indicated influenza strains were exposed to $OSCN^-$ in the cell-free system for 1 h in the presence or absence of catalase, used subsequently to infect MDCK cells, and viral RNA levels were detected by qPCR 6 h postinfection and normalized on host cell GAPDH gene expression. Mean ± S.E.M., n = 3. One-way ANOVA and Tukey's multiple comparisons test. Significance levels are indicated as $*P < 0.05$, $**P < 0.01$, and $***P < 0.001$. Abbreviations: ALI, air–liquid interface; hpi, hours postinfection; IAV, influenza A virus; LPO, lactoperoxidase; NHBE, normal human bronchial epithelial cells; NP, nucleoprotein; PFU, plaque-forming unit; RLU, relative luminescence unit; SCN^-, thiocyanate.

suggest that $OSCN^-$ does not reduce influenza replication by priming host cells before viral challenge and reaffirm the previous observation that $OSCN^-$ specifically (not H_2O_2) inhibits influenza virus.

Viral RNA synthesis is an essential stage of the replication process and can be detected a few hours postinfection. To reveal whether $OSCN^-$ affects viral RNA synthesis in host cells, MDCK cells were infected with the five influenza strains studied so far, and the amount of viral RNA was detected 6 h postinfection by real-time PCR. As the results of Fig. 4*H* show, $OSCN^-$ significantly blocked the synthesis of influenza RNA in the case of all strains that were rescued by catalase. The rescue effect of catalase on viral RNA synthesis was more pronounced in the case of influenza A strains compared with B species (Fig. 4*H*). Thus, $OSCN^-$ effectively blocks influenza RNA synthesis in host cells.

The Structure and NA Activity of the Influenza Virus Are Unaffected by $OSCN^-$. Physical damage to the viral envelope has been described as part of the mechanism of antimicrobial peptides (33). We therefore asked whether $OSCN^-$ leads to similar, physical changes in influenza viruses. Three different influenza strains (A/California/07/2009 [H1N1], A/Aichi/2/1968 [H3N2], and B/Florida/4/2006 Yamagata) were exposed to $OSCN^-$ under the conditions of the cell-free experimental system, and viral morphology was examined by transmission electron microscopy. $OSCN^-$ does not cause structural changes in influenza virus morphology as no visible differences could be observed between treatment groups (*SI Appendix*, Fig. S9). Thus, the antiviral mechanism of action of $OSCN^-$ is likely different from that of antimicrobial peptides.

To determine whether $OSCN^-$ has detectable impact on NA, a fluorescent NA enzymatic activity assay was used (34). No substantial inhibitory effect of $OSCN^-$ on NA activity of influenza

virus suspensions was evident for any of the five influenza virus strains tested, in the presence or absence of catalase (*SI Appendix*, Fig. S10*A*). Similarly, $OSCN^-$ had no significant effect on the enzymatic activity of NA when the recombinant enzymes of two different strains [A/Brisbane/02/2018 NA (H1N1) and A/Texas/50/2012 (H3N2) (35)] were used (*SI Appendix*, Fig. S10*B*). The NA inhibitor, oseltamivir, completely inhibited NA activity, as expected (*SI Appendix*, Fig. S10 *A* and *B*). Therefore, these results suggest that NA is unlikely the molecular target of $OSCN^-$.

Influenza Virus Binding and Entry into Host Cells Are Reduced by LPO-Generated $OSCN^-$. To test if $OSCN^-$ disrupts the virus–host receptor interaction mediated by HA (36), a modified hemagglutination inhibition assay was performed using human red blood cells (RBCs) (37, 38). Treatment of influenza with $OSCN^-$ inhibited subsequent hemagglutination that was reversed by catalase (Fig. 5*A*). To confirm this finding in cell cultures, a virus binding assay was performed using influenza A/Aichi/2/1068 (H3N2) tagged with Alexa-488 (39). $OSCN^-$ caused partial inhibition of influenza virus binding to host cells that was reversed by catalase (Fig. 5*B*). These results propose that $OSCN^-$ diminishes influenza binding to host cells.

After binding to host receptors on the cell surface, influenza viruses are taken up into early endosomes, a step that is mediated by HA and is defined here in this work as "viral entry" (40, 41). In subsequent steps, early endosomes mature into late endosomes, and the viral envelope fuses with the endosomal membrane for the successful release of the viral genome (41). This step called "uncoating" is regulated by acidification of the endosomal pH (41, 42). The lowered pH in the endosome will also lead to acidification of the viral lumen that is mediated by the M2 ion channel (41). The low pH induces a conformational change in HA that is needed for the viral envelope–endosomal membrane fusion and for the dissociation of the M1 matrix protein (41). Subsequently, the content of the viral particle including the viral NP and M1 matrix proteins will be released into the cytosol (41). To investigate whether $OSCN^-$ specifically affects endosomal fusion (uncoating), a function of HA (28, 41), a hemolysis assay was utilized (37, 38). This assay measures the ability of the influenza virus to induce membrane fusion and lysis

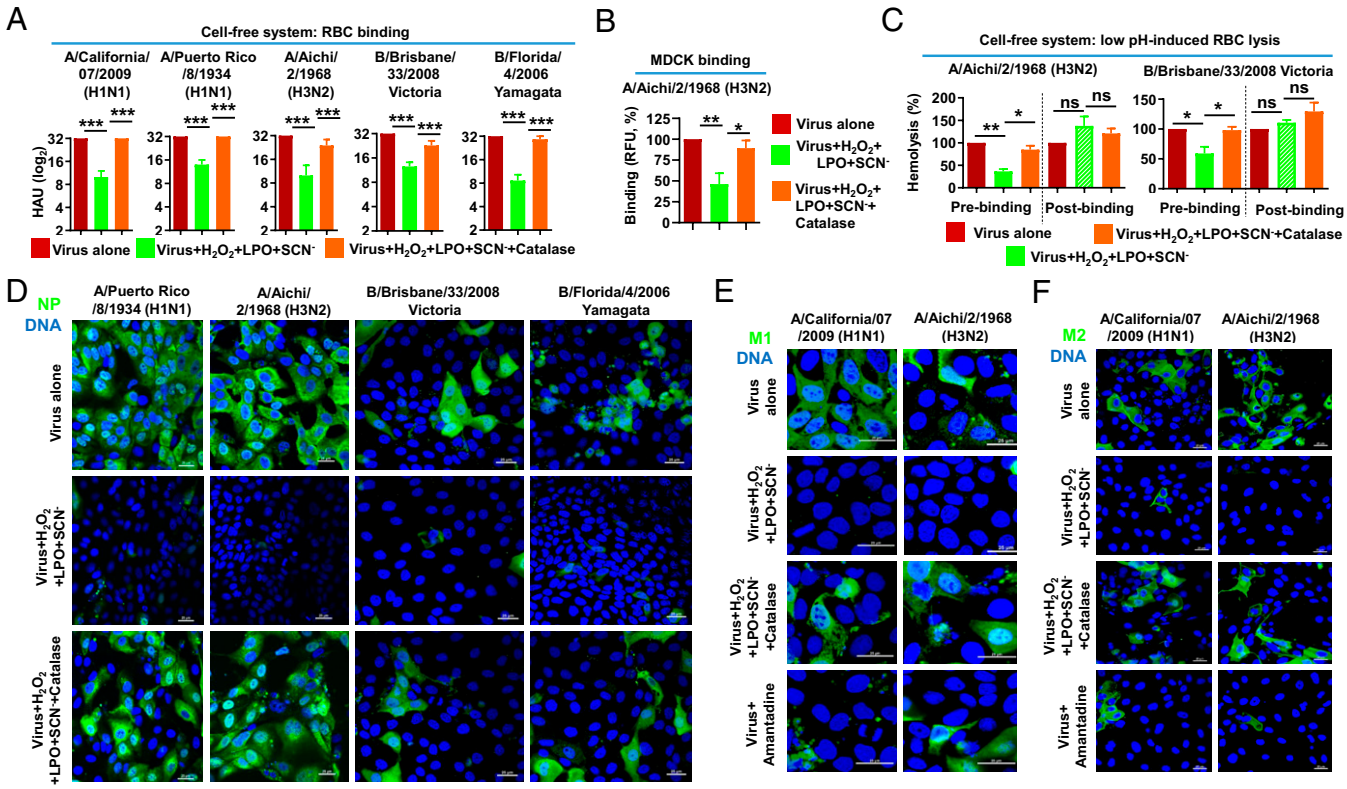

Fig. 5. LPO-generated $OSCN^-$ reduces influenza virus binding and entry into host cells. (*A*) A modified hemagglutination inhibition assay using human RBCs was performed with the indicated influenza virus strains in vitro in the presence of $OSCN^-$, with or without catalase. Data are expressed as mean ± SEM on a $\log_2$ scale of the following numbers of independent experiments: A/California/07/2009 (H1N1) ($n = 6$), A/Puerto Rico/8/1934 (H1N1) ($n = 4$), A/Aichi/2/1968 (H3N2) ($n = 4$), B/Brisbane/33/2008 Victoria ($n = 7$), and B/Florida/4/2006 Yamagata ($n = 6$). One-way ANOVA and Tukey's multiple comparisons tests. (*B*) Attachment of Alexa 488–labeled A/Aichi/2/1968 (H3N2) influenza viruses to MDCK cells was measured in the presence or absence of $OSCN^-$ and catalase as indicated by a fluorescent microplate reader. Data are expressed as a percentage relative to the virus input control and mean ± SEM of $n = 5$ independent experiments performed in triplicates. One-way ANOVA and Tukey's multiple comparisons tests. (*C*) A/Aichi/2/1968 (H3N2) or B/Brisbane/33/2008 Victoria influenza virus strains were exposed to $OSCN^-$ (in presence or absence of catalase) for 1 h in vitro before (prebinding) or after (postbinding) incubation with human RBCs. RBC lysis (hemolysis) indicative of virus-induced endosomal membrane fusion was initiated by lowering the pH and measured as a percentage of untreated controls. Data are expressed as mean ± SEM of $n = 5$ independent experiments performed in triplicates. One-way ANOVA and Tukey's multiple comparisons tests. (*D–F*) The indicated influenza virus strains were allowed to adhere to MDCK cells at 4 °C for 1 h. Unbound virions were washed out, and MDCK cells were exposed to $OSCN^-$ in the presence or absence of catalase for 1 h at 37 °C as indicated. Cells were fixed and subjected to the detection of viral (*D*) NP protein ($n = 3$, 6 hours postinfection [hpi]), (*E*) M1 matrix protein, or (*F*) M2 ion channel ($n = 3$, 3 hpi) by immunofluorescence (green). Host cell DNA was labeled by DAPI (blue). Amantadine was used as a control. Merged images of the viral protein and DAPI-stained nuclei are shown. Images are representative of two or three independent experiments performed in duplicates. (Scale bars, 25 μm.) Significance levels are indicated as $^*P < 0.05$, $^{**}P < 0.01$, and $^{***}P < 0.001$. Abbreviations: HAU, hemagglutination unit; LPO, lactoperoxidase; MDCK, Madin–Darby canine kidney cells; ns, nonsignificant; RBC, red blood cell; RFU, relative fluorescence unit; SCN^-, thiocyanate.

of human RBCs under low pH conditions, independent of its binding to or uptake into RBCs (*SI Appendix*, Fig. S11*A*). Hemolysis indicative of endosomal fusion was unchanged when the influenza virus could bind to RBCs before exposure to $OSCN^-$ (Fig. 5*C* and *SI Appendix*, Fig. S11*A* condition "postbinding"). In contrast, hemolysis was reduced when the virus was first treated with $OSCN^-$ prior to exposure to RBCs (Fig. 5*C*, condition "prebinding"). This suggests that $OSCN^-$ directly affects influenza binding to and entry into host cells.

To further investigate whether $OSCN^-$ affects viral entry and uncoating without binding, influenza virions were allowed to adhere to MDCK cells for 1 h at 4 °C. Unbound virions were washed away, and MDCK cells with virions bound to their surface were exposed to $OSCN^-$, in the presence or absence of catalase, for 1 h at 37 °C under the conditions of the cell-free experimental system. Cells were fixed 3 h later and stained for M1 matrix protein and M2 ion channel indicative of uncoating and for NP 6 h later indicative of nuclear import. The immunofluorescent NP (Fig. 5*D*), M1 (Fig. 5*E*), and M2 (Fig. 5*F*) signals were all lower in MDCK cells exposed to $OSCN^-$ compared with those that were not or also had catalase present (*SI Appendix*, Fig. S11*B*). These results indicate that $OSCN^-$ inhibits postbinding events, as well, primarily viral uptake into host cells.

Proteolytic Cleavage of Hemagglutinin Is Not Affected by LPO-Generated $OSCN^-$. To address whether $OSCN^-$ directly targets HA, recombinant HA (rHA) was exposed to $OSCN^-$, and gel electrophoresis, trypsin protection assay, and ELISAs were performed. No apparent change in the molecular weight of rHA was observed upon exposure to $OSCN^-$ under the conditions of the cell-free experimental system (*SI Appendix*, Fig. S12*A*). Trypsin-mediated cleavage of HA occurs at acidic pH values (41). To address whether $OSCN^-$ would interfere with proteolytic digestion of HA, a trypsin protection assay was used (43). rHA is cleaved in the presence of trypsin and acidic pH (*SI Appendix*, Fig. S12*B*). Proteolytic digestion of rHA of two different influenza strains tested was, however, not affected by prior exposure to $OSCN^-$, in the absence or presence of catalase (*SI Appendix*, Fig. S12*C*). When rHA was probed with characterized antibodies that recognize specific HA head and stem epitopes by ELISA (44, 45), $OSCN^-$ or catalase did not affect these antibody-specific sites as the targets of the antiviral action of $OSCN^-$ (*SI Appendix*, Fig. S12*D*). In summary, $OSCN^-$ does not directly affect the molecular weight of HA or interfere with the action of proteases on HA.

Discussion

Our results show that Duox1 has an essential role in antiviral innate immunity in vivo, and $OSCN^-$ generated by the concerted action of Duox1 and LPO interferes with influenza virus binding and entry into the epithelium. *Duox1*$^{-/-}$ mice are more susceptible to influenza airway challenge than Duox1-expressing mice. Duox1 improves airway epithelial viral clearance, shapes the early antiviral innate response, and reduces infection-related mortality. While Duox1 was discovered in 2000 (2) and its role in $OSCN^-$ generation and LPO partnership was proposed in 2003 (3), this study demonstrates the antimicrobial function of Duox1 in vivo. Prior in vivo studies reported associations of Duox1 with the pathogeneses of several diseases including allergic asthma and chronic obstructive pulmonary disease and with the function of uroepithelial cells (1, 46–48). Our study identifies the in vivo physiological role of Duox1 and shows that Duox1 activity is beneficial to the host response against viral infection. Our results suggest that Duox1 is an underappreciated, important component of the innate immune arsenal of airway epithelial cells against influenza. Since $OSCN^-$ is an oxidant known to kill or inactivate several bacterial and viral pathogens in vitro (13), Duox1 potentially supports the innate immune response against other respiratory pathogens, as well. Duox1 deficiency did not affect other components of this antimicrobial system in vivo that further confirms that Duox1-derived H_2O_2 is the last, most labile component of the LPO/SCN^-/Duox1/H_2O_2 antimicrobial system, as it was proposed originally (3). Regulating Duox1 protein expression or enzymatic activity is likely the on/off switch for this antiviral mechanism. Interestingly, Duox1 was found to be associated with increased levels of several cytokines in the lung 3 d following influenza challenge, especially IL-1β, CCL27, and CXCL5. IL-1β is a major proinflammatory cytokine released primarily by macrophages but to a lower extent also by other cell types including respiratory epithelial cells (49). Influenza lung infection leads to rapid inflammasome activation and IL-1β release that helps establish $CD8^+$ T cell responses, B cell secretion of IgA, and development of helper CD4+ T cells by the regulation of Th17 and Th1 responses (49, 50). Therefore, exploring the direct or indirect connection between Duox1 and IL-1β/inflammasomes could benefit our understanding of the innate and adaptive immune responses against influenza. Duox1 does not directly affect IL-1β secretion in macrophages since we had shown that *Duox1*$^{-/-}$ bone marrow-derived mouse macrophages do not have impaired IL-1β release in response to classical NLPR3 inflammasome agonists in vitro (51). The CCR10 ligand CCL27 is involved in epithelial immunity, mainly in the skin but also at other mucosal sites including the lung, and regulates adaptive immune cell recruitment to mucosal sites (52). Duox1 could affect the adaptive immune response to influenza by promoting CCR10-mediated memory T and B cell migration to the airway epithelium via CCL27 secretion (52). CXCL5 is also known as epithelial-derived neutrophil-activating peptide 78 (ENA-78) that binds to CXCR2 and plays a role in neutrophil recruitment to the airways and their activation under different infectious or inflammatory conditions (53–55). While there was a slight, nonsignificant decrease in neutrophil numbers at 3 dpi in *Duox1*$^{-/-}$ mice compared with WT animals, Duox1-mediated CXCL5 release could drive neutrophil recruitment to influenza-infected airways earlier than 3 dpi. It remains to be determined whether Duox1 directly affects the airway epithelial generation of the affected cytokines or only indirectly via extraepithelial mechanisms, but direct epithelial involvement of Duox1 is likely since the production of several cytokines and chemokines including the ones listed here are known to be promoted by hypoxia or reactive oxygen species (50, 56). Duox1 also increases BAL levels of CCL1, CCL3, CCL11, CCL19, CCL20, and CXCL11 at 3 dpi. These chemokines recruit and activate different immune cells including neutrophils, monocytes, dendritic cells, eosinophils, and lymphocytes during inflammation to the airways, and their levels are influenced by the oxidative status of the cell (56). The only cytokine whose BAL levels were negatively affected by Duox1 is IFN-λ. Type III IFNs are mainly produced by respiratory epithelial cells in the airways and play a crucial role in the rapid, innate immune response to respiratory viral infections including influenza (57). ROS and Duox2 have been previously linked to IFN-λ production during influenza infection (58, 59). It is possible that Duox1-mediated early innate immune responses provide an alternate pathway to mechanisms mediated by Duox2 and IFN-λ upon respiratory viral infection. While Duox1 affected several chemokines at 3 dpi, it had no significant overall effect on BAL levels of the myeloid or lymphoid cells studied at 3 dpi. Although they did not reach the level of significance, BAL numbers of inflammatory monocytes and macrophages at 3 dpi were higher in WT mice than in *Duox1*$^{-/-}$ animals suggesting that the major manifestation of Duox1-promoted chemokine levels in the airways is enhanced monocyte/macrophage recruitment. Indeed, several of the chemokines discussed above are known to recruit these cells to the airways under inflammatory conditions. Interestingly, BAL levels of inflammatory macrophages at 5 dpi were higher in *Duox1*$^{-/-}$ mice. This could be due to a delayed and exaggerated inflammatory response in *Duox1*$^{-/-}$ airways that is mediated by increased viral titers, altered chemokine levels, or both. The levels of chemokines altered by Duox1 at 3 dpi could be even more

affected at 1 and 2 dpi potentially influencing BAL levels of immune cells at earlier time points.

The results shown here support that DUOX1 is the main source of H_2O_2 fueling the antiviral action of $OSCN^-$ in human tracheobronchial epithelial cells (21, 22). SCN^- (3, 60, 61) is transported from the blood into tissues through the airway epithelium (62, 63). Duox1 has its highest expression in respiratory epithelial cells in the lung and provides H_2O_2; the last and most labile component of the system needed for $OSCN^-$ generation in the airway surface liquid (3).

The repertoire of influenza strains susceptible to $OSCN^-$ has been further extended in this work and suggests that $OSCN^-$ works in a strain-independent manner, unlike vaccines (21, 22). The A/Aichi/2/1968 (H3N2) influenza virus strain was less susceptible to $OSCN^-$-mediated inactivation than the other strains tested. This observation is in line with our prior published results showing that H3N2 influenza A viruses are more resistant to $OSCN^-$ than H1N1 influenza A viruses or B strains (22). The exact reason for this pattern remains to be determined but it is likely associated with HA structure. Data presented here suggest that $OSCN^-$ also inactivates an influenza strain resistant to a currently used NA inhibitor, oseltamivir (28). Since emerging resistance to NA inhibitors is a clinically relevant problem, novel alternative approaches are urgently needed to develop new antiviral drugs (29). $OCSN^-$ could provide an attractive, alternative, replacement or complimentary strategy to combat influenza due to its virus strain-independent virucidal activity and safe nature. $OSCN^-$ will be further tested on additional influenza strains resistant to NA or M2 channel inhibitors (64).

Since $OSCN^-$ has antimicrobial activities against numerous pathogens in vitro [most recently reviewed here (13)], and the data reported here show that Duox1 supports the immune response against influenza in vivo, we speculate that Duox1-mediated innate immunity of the lung does not specifically target influenza, but it has a much wider pathogen target repertoire, potentially also including the causative agent of the current pandemic, SARS-CoV-2, that causes coronavirus disease 2019 (COVID-19) (65). SARS-CoV-2 is an airway pathogen that targets respiratory epithelial cells, the cell type expressing Duox1, to initiate infection (66). In fact, it has recently been shown that $OSCN^-$ exhibits virucidal activity against SARS-CoV-2 in vitro (67). Thus, the innate immune mechanisms revealed here likely do not only target influenza viruses but other respiratory pathogens including SARS-CoV-2, as well.

It has remained unknown which molecules or events in the infection cycle of any pathogen are directly targeted by $OSCN^-$ to confer its antimicrobial effects. Previous research proposed that bacterial thioredoxin reductase is a target of $OSCN^-$ (68), but no studies investigated this in viruses. Our results show that $OSCN^-$ targets the influenza virus, and it does not affect the airway epithelium to exert its antiviral action. $OSCN^-$ acts as a direct antimicrobial agent and does not prime antiviral defenses of the host as IFNs do. We also show that extracellular exposure of influenza virus to $OSCN^-$ significantly reduces viral proliferation, RNA synthesis, nuclear translocation, uncoating, and binding in host cells. We propose that $OSCN^-$ directly targets influenza viruses and attenuates the infection cycle by primarily inhibiting viral binding and entry in host cells. We also show that $OSCN^-$ does not influence virion morphology or NA enzymatic activity and does not lead to changes in HA molecular weight, in well-characterized HA surface epitopes or its trypsin sensitivity. Additional research is needed to identify the exact molecular mechanism that $OSCN^-$ uses to prevent influenza binding. Knowledge that $OSCN^-$ acts primarily on reduced cysteines suggests that cysteine residues in one or more influenza proteins, possibly HA, may be the critical target(s) (69, 70).

In summary, our results present evidence for an antiviral role of *Duox1* in influenza infection in vivo. $OSCN^-$ generated by LPO and Duox1-derived H_2O_2 attenuates influenza infection–related mortality, morbidity, and lung viral titers. $OSCN^-$ directly targets influenza virus and decreases its binding and entry into host cells leading to reduced infectivity. In addition to its direct antiviral effect by fueling $OSCN^-$ generation, Duox1 could have an additional, important role in epithelial cytokine release during influenza virus infection. Treatment options for influenza virus infections are limited due to antiviral drug resistance, and strain-specific vaccination is problematic due to the rapidity by which the virus changes. Enhancing the activity of innate immune responses, such as the Duox1/LPO-based mechanism, could provide broader antiviral protection and offer antiviral, disease intervention strategies.

Materials and Methods

Human Subjects. All the human subject studies were performed by following the guidelines of the World Medical Association's Declaration of Helsinki. Healthy human subjects were recruited at the University of Georgia Clinical Translational and Research Unit to donate blood for RBC isolation. The human blood protocol (University of Georgia [UGA] no. 2012-10769-06), the consent form, and the questionnaire were reviewed and approved by the Institutional Review Board of the University of Georgia. Enrolled healthy volunteers provided informed consent before blood draw.

The Institutional Animal Care and Use Committee of the University of Georgia approved all the protocols and procedures used in the animal experiments: A2017 07-010-Y2-A1. *SI Appendix* contains a detailed description of the used cells, animals, human blood cells, and the following protocols: ELISA, electron microscopy, immune cell phenotyping by flow cytometry, histopathology evaluation, trypsin protection assay, sodium dodecyl sulphate–polyacrylamide gel electrophoresis (SDS-PAGE) and Western blot, PCR, immunofluorescence, apoptosis assays, virus propagation and purification, hemagglutination, binding and entry assays, hemolysis measurement, NA assay, and thiocyanate measurements.

Data Availability. All study data are included in the article and/or *SI Appendix*.

ACKNOWLEDGMENTS. This work was supported by the NIH (grants R21AI124189-01A1 to B.R and R.A.T. and R01AI146857-01A1 to B.R. and R.A.T.), the UGA Office of Vice President for Research (startup funds to B.R.), and the Georgia Research Alliance (R.A.T.). We thank Miklós Geiszt (Semmelweiss University, Budapest, Hungary) and Lexicon Pharmaceuticals for providing the *Duox1*$^{-/-}$ mouse strain. The bioluminescent influenza virus strain A/Puerto Rico/8/1934-PA-NanoLuciferase was kindly provided by Andrew Mehle (University of Wisconsin–Madison). The following reagents were obtained through Biodefense and Emerging Infections Research Resources Repository (BEI Resources), National Institute of Allergy and Infectious Diseases (NIAID), NIH: monoclonal anti-influenza virus H1 hemagglutinin protein (clone CA09-02), A/California/04/2009 (H1N1) pdm09, (ascites, mouse), and NR-28665. We thank Jamie Barber, College of Veterinary Medicine flow cytometry core facility manager, for his technical assistance in multicolor flow cytometry and the immunofluorescence imaging. We also thank Mary Brown Ard, coordinator at the Georgia Electron Microscopy Core Facility at the University of Georgia, for her help with electron microscopy. We are also thankful to UGA collaborators Thomas M. Krunkosky, Stephen Mark Tompkins, Jacklyn Crabtree, Cheryl A. Jones, Jarod Hanson, and Daniel Dlugolenski for their help with viral propagation, assay establishment, or experimental troubleshooting.

1. N. M. Ashtiwi, D. Sarr, B. Rada, DUOX1 in mammalian disease pathophysiology. *J. Mol. Med. (Berl.)*, 10.1007/s00109-021-02058-2 (2021).
2. X. De Deken *et al*., Cloning of two human thyroid cDNAs encoding new members of the NADPH oxidase family. *J. Biol. Chem.* **275**, 23227–23233 (2000).
3. M. Geiszt, J. Witta, J. Baffi, K. Lekstrom, T. L. Leto, Dual oxidases represent novel hydrogen peroxide sources supporting mucosal surface host defense. *FASEB J.* **17**, 1502–1504 (2003).
4. S. Morand *et al*., Duox maturation factors form cell surface complexes with Duox affecting the specificity of reactive oxygen species generation. *FASEB J.* **23**, 1205–1218 (2009).
5. B. Rada, H. E. Boudreau, J. J. Park, T. L. Leto, Histamine stimulates hydrogen peroxide production by bronchial epithelial cells via histamine H1 receptor and dual oxidase. *Am. J. Respir. Cell Mol. Biol.* **50**, 125–134 (2014).
6. B. Rada, K. Lekstrom, S. Damian, C. Dupuy, T. L. Leto, The Pseudomonas toxin pyocyanin inhibits the dual oxidase-based antimicrobial system as it imposes oxidative stress on airway epithelial cells. *J. Immunol.* **181**, 4883–4893 (2008).
7. G. E. Conner, M. Salathe, R. Forteza, Lactoperoxidase and hydrogen peroxide metabolism in the airway. *Am. J. Respir. Crit. Care Med.* **166**, S57–S61 (2002).

8. G. E. Conner, C. Wijkstrom-Frei, S. H. Randell, V. E. Fernandez, M. Salathe, The lactoperoxidase system links anion transport to host defense in cystic fibrosis. *FEBS Lett.* **581**, 271–278 (2007).
9. C. Gerson *et al*., The lactoperoxidase system functions in bacterial clearance of airways. *Am. J. Respir. Cell Mol. Biol.* **22**, 665–671 (2000).
10. C. Wijkstrom-Frei *et al*., Lactoperoxidase and human airway host defense. *Am. J. Respir. Cell Mol. Biol.* **29**, 206–212 (2003).
11. P. Z. Allen, M. Morrison, V. I. Lactoperoxidase, Lactoperoxidase. VI. Immunochemical studies on lactoperoxidase from the milk of several species. *Arch. Biochem. Biophys.* **113**, 540–547 (1966).
12. A. S. Goldman, C. W. Smith, Host resistance factors in human milk. *J. Pediatr.* **82**, 1082–1090 (1973).
13. D. Sarr, E. Tóth, A. Gingerich, B. Rada, Antimicrobial actions of dual oxidases and lactoperoxidase. *J. Microbiol.* **56**, 373–386 (2018).
14. J. D. Chandler, B. J. Day, Thiocyanate: A potentially useful therapeutic agent with host defense and antioxidant properties. *Biochem. Pharmacol.* **84**, 1381–1387 (2012).
15. P. Moskwa *et al*., A novel host defense system of airways is defective in cystic fibrosis. *Am. J. Respir. Crit. Care Med.* **175**, 174–183 (2007).
16. C. Dupuy *et al*., Purification of a novel flavoprotein involved in the thyroid NADPH oxidase. Cloning of the porcine and human cDNAs. *J. Biol. Chem.* **274**, 37265–37269 (1999).
17. J. D. Chandler *et al*., Antiinflammatory and antimicrobial effects of thiocyanate in a cystic fibrosis mouse model. *Am. J. Respir. Cell Mol. Biol.* **53**, 193–205 (2015).
18. J. D. Chandler, E. Min, J. Huang, D. P. Nichols, B. J. Day, Nebulized thiocyanate improves lung infection outcomes in mice. *Br. J. Pharmacol.* **169**, 1166–1177 (2013).
19. H. Buvelot, V. Jaquet, K. H. Krause, Mammalian NADPH oxidases. *Methods Mol. Biol.* **1982**, 17–36 (2019).
20. J. Dunning, R. S. Thwaites, P. J. M. Openshaw, Seasonal and pandemic influenza: 100 years of progress, still much to learn. *Mucosal Immunol.* **13**, 566–573 (2020).
21. A. Gingerich *et al*., Hypothiocyanite produced by human and rat respiratory epithelial cells inactivates extracellular H1N2 influenza A virus. *Inflamm. Res.* **65**, 71–80 (2016).
22. U. Patel *et al*., Susceptibility of influenza viruses to hypothiocyanite and hypoiodite produced by lactoperoxidase in a cell-free system. *PloS One* **13**, e0199167 (2018).
23. A. Donkó, Z. Péterfi, A. Sum, T. Leto, M. Geiszt, Dual oxidases. *Philos. Trans. R. Soc. Lond. B Biol. Sci.* **360**, 2301–2308 (2005).
24. X. De Deken, D. Wang, J. E. Dumont, F. Miot, Characterization of ThOX proteins as components of the thyroid H(2)O(2)-generating system. *Exp. Cell Res.* **273**, 187–196 (2002).
25. A. García-Sastre, C. A. Biron, Type 1 interferons and the virus-host relationship: A lesson in détente. *Science* **312**, 879–882 (2006).
26. D. Fujikura, T. Miyazaki, Programmed cell death in the pathogenesis of influenza. *Int. J. Mol. Sci.* **19**, 2065 (2018).
27. A. D. Gingerich *et al*., Oxidative killing of encapsulated and nonencapsulated *Streptococcus pneumoniae* by lactoperoxidase-generated hypothiocyanite. *PloS One* **15**, e0236389 (2020).
28. M. von Itzstein, The war against influenza: Discovery and development of sialidase inhibitors. *Nat. Rev. Drug Discov.* **6**, 967–974 (2007).
29. M. Samson, A. Pizzorno, Y. Abed, G. Boivin, Influenza virus resistance to neuraminidase inhibitors. *Antiviral Res.* **98**, 174–185 (2013).
30. Y. Abed, A. Pizzorno, X. Bouhy, C. Rhéaume, G. Boivin, Impact of potential permissive neuraminidase mutations on viral fitness of the H275Y oseltamivir-resistant influenza A(H1N1)pdm09 virus in vitro, in mice and in ferrets. *J. Virol.* **88**, 1652–1658 (2014).
31. M. B. Grisham, E. M. Ryan, Cytotoxic properties of salivary oxidants. *Am. J. Physiol.* **258**, C115–C121 (1990).
32. E. A. Karlsson *et al*., Measuring influenza virus infection using bioluminescent reporter viruses for in vivo imaging and in vitro replication assays. *Methods Mol. Biol.* **1836**, 431–459 (2018).
33. S. H. Lee *et al*., The amphibian peptide Yodha is virucidal for Zika and dengue viruses. *Sci. Rep.* **11**, 602 (2021).
34. A. J. Mooney *et al*., Vaccination with recombinant parainfluenza virus 5 expressing neuraminidase protects against homologous and heterologous influenza virus challenge. *J. Virol.* **91**, e01579-17 (2017).
35. J. W. Ecker *et al*., High-yield expression and purification of recombinant influenza virus proteins from stably-transfected mammalian cell lines. *Vaccines (Basel)* **8**, 462 (2020).
36. L. Byrd-Leotis, R. D. Cummings, D. A. Steinhauer, The interplay between the host receptor and influenza virus hemagglutinin and neuraminidase. *Int. J. Mol. Sci.* **18**, 1541 (2017).
37. T. J. Lin, C. F. Lin, C. H. Chiu, M. C. Lee, J. T. Horng, Inhibition of endosomal fusion activity of influenza virus by Rheum tanguticum (da-huang). *Sci. Rep.* **6**, 27768 (2016).
38. L. Zhu *et al*., Inhibition of influenza A virus (H1N1) fusion by benzenesulfonamide derivatives targeting viral hemagglutinin. *PloS One* **6**, e29120 (2011).
39. L. Byrd-Leotis *et al*., Shotgun glycomics of pig lung identifies natural endogenous receptors for influenza viruses. *Proc. Natl. Acad. Sci. U.S.A.* **111**, E2241–E2250 (2014).
40. N. J. Overeem, E. van der Vries, J. Huskens, A dynamic, supramolecular view on the multivalent interaction between influenza virus and host cell. *Small* **17**, e2007214 (2021).
41. Y. Yamauchi, Influenza A virus uncoating. *Adv. Virus Res.* **106**, 1–38 (2020).
42. S. Li *et al*., pH-Controlled two-step uncoating of influenza virus. *Biophys. J.* **106**, 1447–1456 (2014).
43. D. De Marco *et al*., A non-VH1-69 heterosubtypic neutralizing human monoclonal antibody protects mice against H1N1 and H5N1 viruses. *PloS One* **7**, e34415 (2012).
44. G. A. Sautto *et al*., A computationally optimized broadly reactive antigen subtype-specific influenza vaccine strategy elicits unique potent broadly neutralizing antibodies against hemagglutinin. *J. Immunol.* **204**, 375–385 (2020).
45. A. L. Skarlupka, Z. B. Reneer, R. B. Abreu, T. M. Ross, G. A. Sautto, An influenza virus hemagglutinin computationally optimized broadly reactive antigen elicits antibodies endowed with group 1 heterosubtypic breadth against swine influenza viruses. *J. Virol.* **94**, e02061-19 (2020).
46. A. Habibovic *et al*., DUOX1 mediates persistent epithelial EGFR activation, mucous cell metaplasia, and airway remodeling during allergic asthma. *JCI Insight* **1**, e88811 (2016).
47. C. Schiffers *et al*., Downregulation of epithelial DUOX1 in chronic obstructive pulmonary disease. *JCI Insight* **6**, e142189 (2021).
48. A. Donkó *et al*., Urothelial cells produce hydrogen peroxide through the activation of Duox1. *Free Radic. Biol. Med.* **49**, 2040–2048 (2010).
49. S. T. Sarvestani, J. L. McAuley, The role of the NLRP3 inflammasome in regulation of antiviral responses to influenza A virus infection. *Antiviral Res.* **148**, 32–42 (2017).
50. I. C. Allen *et al*., The NLRP3 inflammasome mediates in vivo innate immunity to influenza A virus through recognition of viral RNA. *Immunity* **30**, 556–565 (2009).
51. B. Rada, J. J. Park, P. Sil, M. Geiszt, T. L. Leto, NLRP3 inflammasome activation and interleukin-1β release in macrophages require calcium but are independent of calcium-activated NADPH oxidases. *Inflamm. Res.* **63**, 821–830 (2014).
52. N. Xiong, Y. Fu, S. Hu, M. Xia, J. Yang, CCR10 and its ligands in regulation of epithelial immunity and diseases. *Protein Cell* **3**, 571–580 (2012).
53. J. Mei *et al*., Cxcr2 and Cxcl5 regulate the IL-17/G-CSF axis and neutrophil homeostasis in mice. *J. Clin. Invest.* **122**, 974–986 (2012).
54. Y. Liang *et al*., Role of neutrophil chemoattractant CXCL5 in SARS-CoV-2 infection-induced lung inflammatory innate immune response in an in vivo hACE2 transfection mouse model. *Zool. Res.* **41**, 621–631 (2020).
55. L. A. Sokulsky *et al*., A critical role for the CXCL3/CXCL5/CXCR2 neutrophilic chemotactic axis in the regulation of type 2 responses in a model of rhinoviral-induced asthma exacerbation. *J. Immunol.* **205**, 2468–2478 (2020).
56. J. Korbecki *et al*., The effect of hypoxia on the expression of CXC chemokines and CXC chemokine receptors-A review of literature. *Int. J. Mol. Sci.* **22**, 843 (2021).
57. A. A. Lozhkov *et al*., The key roles of interferon lambda in human molecular defense against respiratory viral infections. *Pathogens* **9**, 989 (2020).
58. H. J. Kim *et al*., Reactive oxygen species induce antiviral innate immune response through IFN-λ regulation in human nasal epithelial cells. *Am. J. Respir. Cell Mol. Biol.* **49**, 855–865 (2013).
59. B. J. Kim *et al*., Intranasal delivery of Duox2 DNA using cationic polymer can prevent acute influenza A viral infection in vivo lung. *Appl. Microbiol. Biotechnol.* **102**, 105–115 (2018).
60. D. E. Heppner *et al*., The NADPH oxidases DUOX1 and NOX2 play distinct roles in redox regulation of epidermal growth factor receptor signaling. *J. Biol. Chem.* **291**, 23282–23293 (2016).
61. A. W. Boots *et al*., ATP-mediated activation of the NADPH oxidase DUOX1 mediates airway epithelial responses to bacterial stimuli. *J. Biol. Chem.* **284**, 17858–17867 (2009).
62. M. A. Fragoso, A. Torbati, N. Fregien, G. E. Conner, Molecular heterogeneity and alternative splicing of human lactoperoxidase. *Arch. Biochem. Biophys.* **482**, 52–57 (2009).
63. N. Pedemonte *et al*., Thiocyanate transport in resting and IL-4-stimulated human bronchial epithelial cells: Role of pendrin and anion channels. *J. Immunol.* **178**, 5144–5153 (2007).
64. S. E. Mtambo *et al*., Influenza viruses: Harnessing the crucial role of the M2 ion-channel and neuraminidase toward inhibitor design. *Molecules* **26**, 880 (2021).
65. T. P. Velavan, C. G. Meyer, The COVID-19 epidemic. *Trop. Med. Int. Health* **25**, 278–280 (2020).
66. G. Ryu, H. W. Shin, SARS-CoV-2 infection of airway epithelial cells. *Immune Netw.* **21**, e3 (2021).
67. L. Cegolon *et al*., Hypothiocyanite and hypothiocyanite/lactoferrin mixture exhibit virucidal activity in vitro against SARS-CoV-2. *Pathogens* **10**, 233 (2021).
68. J. D. Chandler, D. P. Nichols, J. A. Nick, R. J. Hondal, B. J. Day, Selective metabolism of hypothiocyanous acid by mammalian thioredoxin reductase promotes lung innate immunity and antioxidant defense. *J. Biol. Chem.* **288**, 18421–18428 (2013).
69. O. Skaff, D. I. Pattison, M. J. Davies, Hypothiocyanous acid reactivity with low-molecular-mass and protein thiols: Absolute rate constants and assessment of biological relevance. *Biochem. J.* **422**, 111–117 (2009).
70. J. D. Chandler, B. J. Day, Biochemical mechanisms and therapeutic potential of pseudohalide thiocyanate in human health. *Free Radic. Res.* **49**, 695–710 (2015).